ASTM E659 Standardized Test Analysis and Results for Synthetic Paraffinic Kerosene

Charline Fouchier[a,b] & Joseph Shepherd[a]

[a] Graduate Aerospace Laboratories, California Institute of Technology, Pasadena, CA, USA
[b] von Karman Institute for Fluid Dynamics, Sint Genesius Rode, Belgium

E-mail: *charline@caltech.edu*

Abstract

Improvements on ASTM E659 apparatus are used to investigate autoignition (AIT) of a Synthetic Paraffinic Kerosene (SPK). The apparatus injection system has been automated, and the temperature acquisition system has been improved to reduce variability due to human factors. The SPK was compared with a Jet A standard, POSF4658. The two fuels have a similar range of combustion behaviors but the SPK shows a lower AIT and lower effective activation energy than Jet A. A statistical analysis is proposed to quantify the likelihood of ignition for a range of injected fuel volumes and types of ignition events. We observe that luminous ignition (Mode I) and non-luminous cool flame (Mode III) both result in a vigorous reaction and comparable peak temperatures. This highlights the importance of using the temperature signal to detect ignition instead of relying only on flame visualization. Surveys of the temperature distribution inside the hot vessel demonstrate that a single point measurement is not sufficient to characterize the temperature and that subtle changes in the assembly of the apparatus can significantly alter the temperature distribution and the measured AIT.

Keywords: *Thermal Ignition, Flammability, Standardized Tests, Synthetic Paraffinic Kerosene, Safety*

1 Introduction

The ignition of flammable gases, combustible liquids, or powders in a hot air atmosphere is a critical safety concern in many industries such as power generation, petroleum, automotive, chemical, and aerospace. In order to evaluate the hazard of ignition, standardized tests have been developed to determine a temperature threshold, the autoignition temperature (AIT). The AIT is defined as the minimum temperature required to initiate self-sustaining combustion in the absence of an external source of ignition such as a spark or flame (NFPA, 1991). The AIT, as defined by standardized tests, is widely used to define maximum safe operating temperatures for surfaces in the presence of flammable or combustible substances.

However, the standard AIT test is not a hot surface test but examines the case of a hot flammable atmosphere surrounded by a hot surface in a confined geometry. While this is an important test for hazard evaluation, particularly the classical self-heating or thermal runaway condition (Semenoff, 1929, Frank-Kamenetskii, 2015), many hazards involve hot surfaces surrounded by a cold atmosphere with an unconfined geometry (Jones and Shepherd, 2021) and the ignition threshold surface temperatures in the latter case can be much higher (500-600°C) than the standard test AIT values. In the present study, we focus exclusively on the self-heating aspect of autoignition in a confined hot atmosphere within a hot vessel.

The most widely used methodologies for determining AIT are ASTM-E659 (2005) standard and the international standard (ISO/IEC (2017)). In our study, we have used the ASTM apparatus. The protocol consists of injecting a small fuel quantity into a 500 mL rounded bottom flask heated at a constant temperature in a furnace and observing for 10 minutes the presence or absence of flame. Following a specific procedure for varying the temperature and fuel volume in the test, a minimum temperature at which the ignition occurs is used to specify the AIT.

The current standardized test apparatus and protocols evolved from substantial prior work in the twentieth century. Setchkin (1954) *et al.* developed an early version, gave results for various fuels,

and provided a comprehensive summary of testing methods being used at that time. They highlighted important parameters affecting the AIT, which have been the focus of many studies since that time. They found that the AIT becomes lower with increasing vessel size, and the ratio of the combustible substance to air was a significant factor. Setchkin also emphasized the importance of temperature uniformity inside the flask and the difficulties in observing the flame during ignition in some cases, advising the analysis of the temperature signal rather than purely visual observation.

Other factors known to influence the AIT include the shape of the flask, the rate and duration of heating, and the flask material (NFPA (1991)). Recent studies have examined further the effect of the combustion vessel and the influence of increased pressure and nitrogen dilution levels on the AIT (Hirsch and Brandes, 2005, Brandes et al., 2018). The effect of the flask material has been highlighted by Chen and Hsieh (2010) where the AIT of ethanol measured inside a quartz flask was found to be 20 °C higher than the one measured in a borosilicate flask. The same authors investigated the effect of the ambient temperature and found a quadratic relation between the AIT and the ambient temperature, where the AIT showed an increase of around 10 °C for an increase of 25°C on the ambient temperature. The cleanliness of the flask was also reported to affect the AIT (Martin (2023)), where a flask used multiple times can lead to higher AIT readings.

While the ASTM standard defines ignition with the presence of a flame, it has been frequently reported that ignition could lead to a weak flame that can be invisible to human eyes. Many authors recommend detecting ignition based on the temperature signal rise instead of the flame visualization (Affens et al., 1961, Johnson and Mashuga, 2023, Setchkin, 1954). This difference in definition leads to significant variation in the reported AIT value. Over time, different ignition modes have appeared, such as the four ignition modes used by Martin and Shepherd (2021), and can be used to qualitatively take into account the complexity of ignition. The ASTM standard does not describe the injection rate and height of injection, while the evaporation rate has been shown to have a non-negligible effect on the AIT (Swarts and Orchin (1957)). Finally, fluid motion and mixing have been shown to affect the autoignition (Mastorakos et al., 1997, Martin, 2023). The standard states that the flask temperature should be uniform, but measuring the temperature distribution and quantifying uniformity is not part of the standard.

The main objectives of this work are to report some improvement in the apparatus, provide data on a new fuel, a synthetic paraffinic kerosene, to raise awareness about the challenges of using the ASTM protocol when characterizing a new fuel, and propose some new statistical methods of analyzing test data to account for a range of compositions. Tests have been conducted under conditions similar to the standard protocol, and we identified some limitations as well as proposed improvements to reduce the measurement uncertainties. The paper is organized as follows. Section 2 gives the experimental details, including modifications to the ASTM apparatus, the experimental procedure, and the tested fuels. Two fuels are tested in the present project: Jet A POSF-4658, also tested by Martin and Shepherd (2021), and a representative Synthetic Paraffinic Kerosene (SPK). Section 3 gathers the experimental results. The first subsection discusses the test repeatability. The second subsection gives the ignition maps and compares results for the two fuels. The difference between Mode I (flame) and Mode III (no flame) ignition is discussed. The third section investigates the ignition characterization, including an estimation of the effective activation energies of the two fuels, and the maximum temperature measured during ignition. The ignition transition is discussed in the fourth section, while the fifth section gives a statistical analysis of this transition. The sixth subsection discusses the ASTM apparatus and how to estimate a more accurate AIT. Finally, a conclusion and recommendations are given.

2 Experiments

2.1 Experimental setup

The apparatus used by Martin et al. for the characterization of the AIT of Jet A and surrogate jet fuels (Martin and Shepherd (2021), Martin (2023)), constructed based on the ASTM-E659 (2005)

standards, was adapted for this work. Figure 1 is a photograph and a cross-section drawing of the ASTM setup.

The apparatus is composed of a Mellen CV12 crucible furnace with a 133 mm diameter and 200 mm deep cylindrical volume, which heats up at a controlled temperature a 500 mL round bottom borosilicate flask up to 1250°C with a PID controller (Love Controls series 16B) system accurate to 1°C. The flask is suspended in the furnace by a ceramic holder molded from silica-based Cotronics Rescor 750. The flask and the bottom part of the ceramic holder are covered by aluminum foil to reflect the radiation inside the flask and reduce heat loss. A 50 mm diameter mirror is positioned above the apparatus's opening at a 45° angle to allow the user to visualize the flames inside the flask. The fuel injection is made with a 500 μL hypodermic syringe with a 6-inch long (152.4 mm) 26 gauge needle.

The temperature of the flask surface is measured with three thermocouples type K, gauge 34, from Omega, inside a mineral-insulated metal sheath, set at position T1, T2, and T3 (see Figure 1 right). The air temperature is measured with a thermocouple type K, gauge 36, inside a 3 mm diameter ceramic sheath set at T4 in the middle of the flask. The temperature T4 is used as the reference temperature, and has an uncertainty of 0.75 %, with a minimum of 2.2 °C (value provided by the manufacturer).

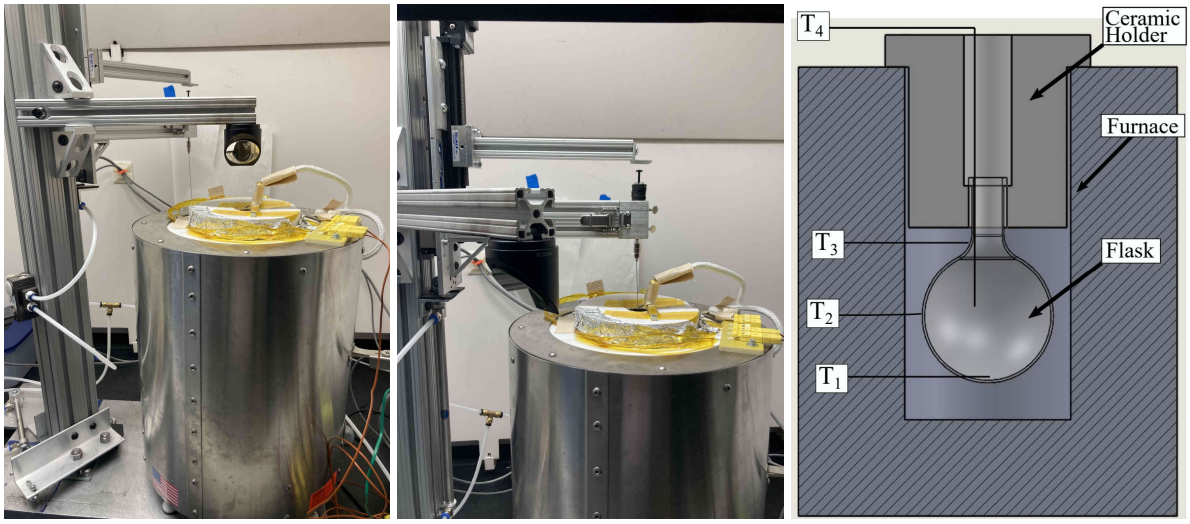

Fig. 1*: (Left) ASTM-E659 test apparatus in visualization mode. (Middle) Apparatus in injection mode with a closer look at the injection system. (Right) Cross-section schematic of the internal heated region with thermocouple locations highlighted.*

The temperature of the flask is not homogeneous and depends on the setup configuration. Two configurations have been used during this project. The two are very similar, with the only difference being that the aluminum foil of Configuration 1 has a discontinuity (gap) between the flask and the ceramic holder, while Configuration 2 does not. A drawing to illustrate the two configurations is given in Figure 2. The gap in the foil increases the flow of hot air in the ceramic holder opposing the counterflow of cold air falling downward toward the flask. This leads to a different temperature profile inside the flask between the two configurations.

The vertical temperature profile over the flask centerline when T4 = 235°C is given in Figure 3 for the two configurations. The temperature has been acquired at 75 Hz for 120 seconds and averaged for each position. A pause of 60 seconds has been made between each position change. The position 0 mm corresponds to the bottom of the flask. Half of the flask's approximate dimensions have been represented in the figure for illustration purposes. In Configuration 1, the temperature increases with height until the middle of the flask neck, after which it decreases. This is due to natural convection, where hot air can circulate around the flask's rounded part and neck. In Configuration 2, the flask temperature is nearly constant up to the 2/3 height of the flask and decreases near the end of the flask

round portion. The flask neck is suspended in the ceramic holder, and the absence of hot air circulation around it leads to a decrease in temperature. Values of the mean temperature over the profile, the difference between the temperature given by T4 and the mean temperature, and the difference between T4 and the profile extrema are given in Table 1. Only points inside the round (bottom) portion of the flask are considered, as ignition occurs in this area. The difference in fluid motion and influence on the temperature profiles is analyzed in detail in a companion publication (Davis et al., 2024). Most of the results discussed in this paper come from Configuration 1, and a few data have been taken in Configuration 2 for comparison purposes.

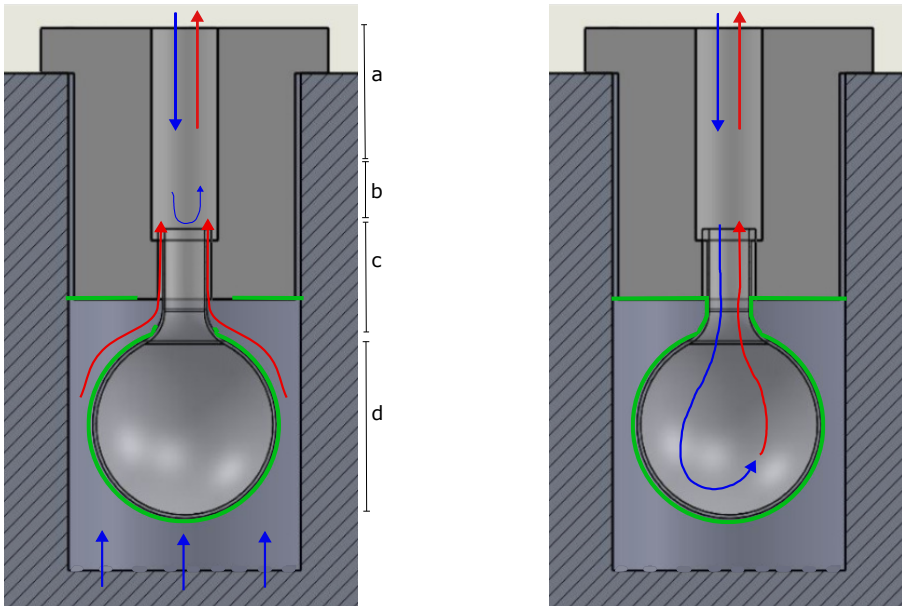

***Fig. 2**: Configuration 1 (Left) and Configuration 2 (Right). Highlighted features: (a) cold and hot air entering and leaving the furnace through the ceramic holder neck, (b) cold air back-flow created by the hot air flowing along the flask neck due to the aluminum foil (green) opening (c), leading to different atmosphere conditions inside the flask (d) compared to Configuration 2.*

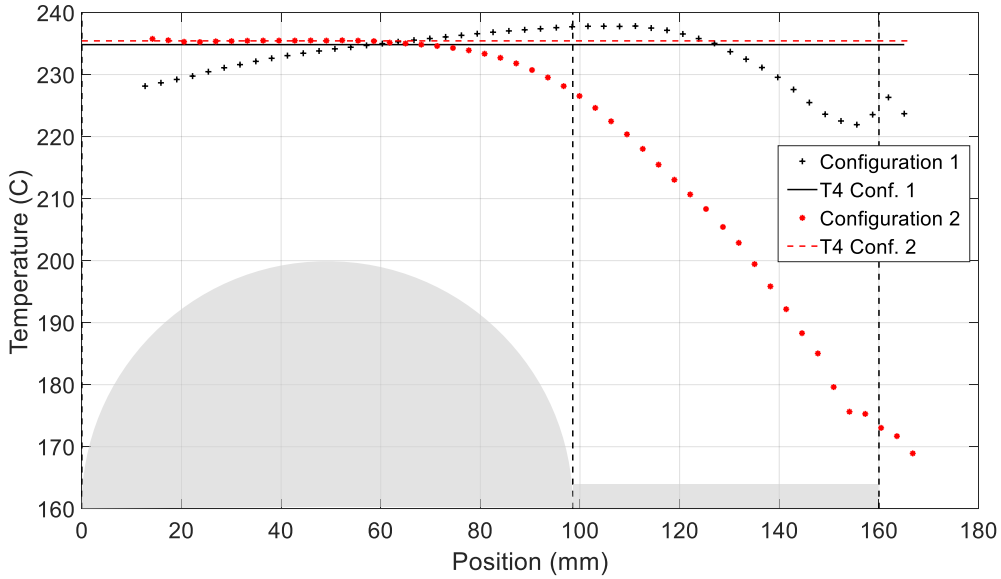

***Fig. 3**: Temperature profile inside the flask for the two configurations, T4 = 235°C*

***Table 1**: Comparison of T4 with flask temperature*

Configuration	T4	T_{mean}	$(T_{mean} - T4)/T4$	$(T_{max} - T_{min})/T4$
Conf. 1	234.8°C	234°C	0.34%	2.8%
Conf. 2	235.4°C	234°C	0.59%	3.8%

The apparatus has been modified from the original design for the sake of the study. First, the temperature variation is recorded with a 16-channel, 24-bit, 75 Hz thermocouple acquisition module (NI 9213) from National Instruments, connected to a cDAQ-9171 CompactDAQ Chassis. The module has one internal autozero channel, 1 internal cold-junction compensation channel, and 16 thermocouple channels. This system allows a higher resolution in time compared to a 1 Hz recorder usually used.

Efforts have been made to improve the fuel injection repeatability and control key parameters, such as the injection velocity, height, and duration. Instead of the manual injection described in the ASTM standards, injection is automated with a Velmex slide (NEMA 17, 115 mm travel) connected to a computer. A vertical stand mounted on a rotating platform holds the syringe and a mirror, allowing the user to switch from the injection to the observation with a 45° rotation. Tests are conducted in Pasadena, California, United States, 260 m above sea level, and the pressure is nominally at 1 atm with small day-to-day variations.

2.2 Experimental methods

The test procedure is as follows. The flask is set at the desired temperature, and thermal stability is reached before each test (variation less than 0.5°C/min). A temperature sample of 30 seconds from T4, in the middle of the flask, is recorded just before the injection, and the average is used as the initial test temperature. Once the measurement is completed, the syringe is lowered to a specified location inside the flask using an air-actuated cylinder. The fuel is injected into the lower part of the flask using the Velmex translation stage to actuate the plunger, the syringe is raised with the air cylinder, and the vertical stand holding the syringe is rotated 45° to place the mirror over the flask opening. The temperature acquisition begins at the same moment as the fuel injection. A test lasts 10 minutes, during which the temperature is recorded, and the presence or absence of flame is observed. After each test, the flask is flushed using a heat gun and an aluminum cylinder. It takes approximately 30 minutes between each test to reach thermal stability.

After a number of tests, particularly with non-ignition events, deposits accumulate on the flask walls, which tends to increase the AIT value (Martin, 2023). The flask is frequently visually inspected and, if necessary, cleaned via a thermal cycle (600°C for 2 hours) or replaced. Examples of flasks used for aviation fuel tests are shown in Figure 4. The left one is an unused flask. The middle one is a flask used for around ten tests with the SPK; this one can be cleaned with a thermal cycle. The right one is a flask used many times with Jet A, and after several thermal cleaning cycles, this one needs to be replaced.

Fuel volumes between 25 to 600 μL ($\pm 5\mu$L) are tested with temperatures T4 from 190 to 280°C ($\pm$2.2°C). Two fuels are examined: a representative Synthetic Paraffinic Kerosene (SPK) and a JetA standard, POSF-4658. The two fuels are described in Section 2.3. The SPK has been tested most extensively using a range of fuel volumes and temperatures. Tests using Jet A fuel have been limited to a few values for comparison with the results of Martin and Shepherd (2021) in order to validate the improved apparatus.

***Fig. 4**: New (left), used (center), heavily used (right) flasks after testing with aviation fuels*

The ignition behaviors are classified into four distinct modes, as used by Martin and Shepherd (2021): (I) Ignition, (II) Cool Flame, (III) Non-Luminous Cool Flame, and (IV) Rapid Reaction. They are defined based on visual observations and temperature variations measured in the middle of the flask (T4). The description of each mode is given in Table 2. The classification is very similar to the one used by Affens et al. (1961), with the addition of Mode II characterized by a small luminosity flame and a small temperature rise. In the present study, this mode is not observed as it primarily occurs in compounds with higher ignition temperatures (>400°C, Martin and Shepherd (2021)).

***Table 2**: Classifications of ignition modes observed in ASTM-E659*

Ignition Mode	Name	Luminosity	Temperature Rise
I	Ignition	Large [a]	Large
II	Cool Flame	Small	Small
III	Non-Luminous Cool Flame	None [b]	Large
IV	Rapid Reaction	None	Small
-	Non-Ignition	None	< 15°C

[a] Associated with a weak to intense explosion sound

[b] None or faint glow only visible to the naked eye, and small puff of smoke

The temperature signals are processed by extracting the maximum temperature recorded and the ignition delay time. The maximum temperature used in this project is measured by the thermocouple T4. It does not represent the flame temperature, which might be higher. Even though the thermocouple is small (36 gauge, 0.127 mm diameter), its size and thermal mass result in a response time that is too slow to capture the flame temperature accurately. However, the thermocouple response is repeatable between tests, and the temperature trace is used as a comparison tool in this work. The ignition delay time corresponds to the moment when the temperature increases the fastest. It is extracted using the peak of the signal second derivative, as illustrated by Figure 5.

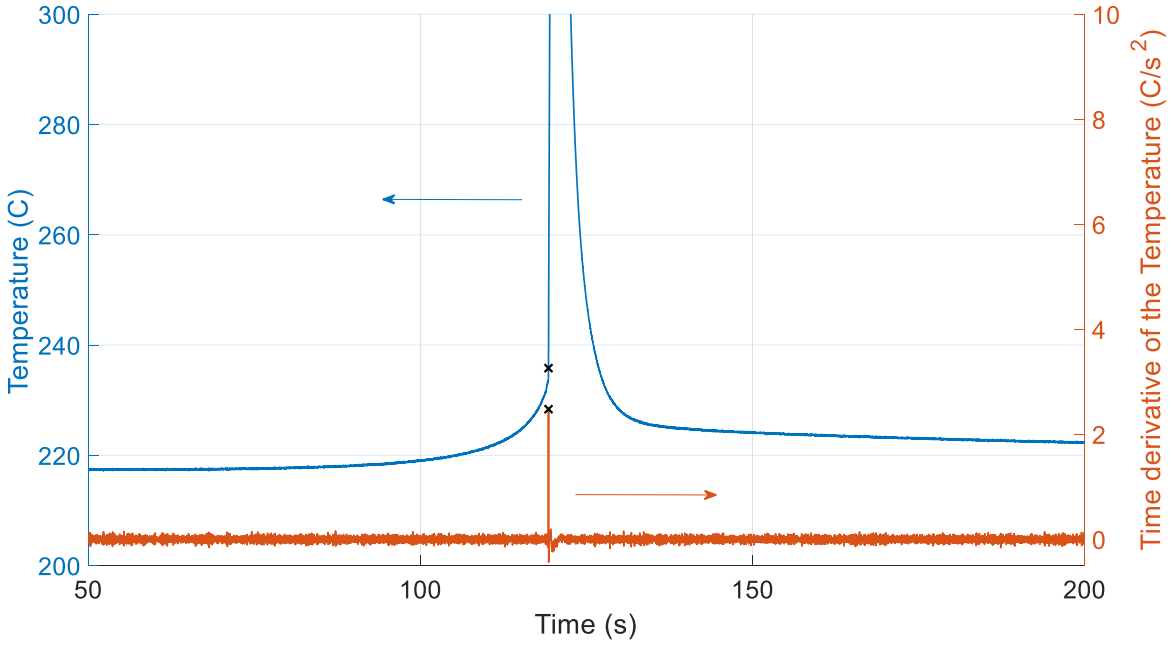

***Fig. 5**: Detection of the ignition beginning using the second derivative of the signal. The ignition delay time is represented by a black cross*

2.3 Tested fuels

Two fuels are used in this work: Jet A POSF-4658, identical to the one used by Martin and Shepherd (2021), and a representative Synthetic Paraffinic Kerosene (SPK). The flask point of the two fuels has been measured following the standard ASTM-D56 (1999) at 46°C for Jet A, and 40°C for the SPK.

An AccuTOF™ GC-Alpha (JEOL, Inc.) Gas Chromatography-Mass Spectrometer (GC-MS) was used to investigate and compare the composition of the two fuels. The GC (Model 8890, Agilent Technologies) was fitted with a Restek Rxi-5ms column with dimensions of 30 m × 0.53 mm i.d. × 1.5 μm film thickness. The GC front inlet temperature was 250°C, and the total He flow was 1 mL/min. 1 μL of sample was injected onto the column with a split ratio of 200 for Field Ionization (FI) MS and 250 for Electron Ionization (EI) MS. The GC run started at 40°C with a 1-minute hold, then raised to 150°C with a gradient of 2°C/min and 30°C/min up to 300°C with a 1-minute hold. The total analysis time was 62 minutes. During the last two minutes of each run, an Octamethylcyclotetrasiloxane standard (Aldrich, m/z = 281.05114) was introduced into the ion source for mass-scale drift compensation. Mass spectra were acquired by Field Ionization (FI), which generates molecular ions, and Electron Ionization (EI), which generates diagnostic fragment ions allowing full characterization of the sample components. The FI signals of the SPK and Jet A are given respectively in Figures 6 and 7. Each peak can be associated with a particular molecule by combining the FI and the EI signals. This analysis has been done automatically with the msFineAnalysis AI software (msFineAnalysis, 2023) for all the detected peaks. Some molecules have been added to the figures to highlight the differences and similarities between the two fuels. All stronger peaks are due to linear alkanes for Jet A, and linear and iso-alkanes for SPK. SPK does not have any aromatic molecules, Jet A has multiple peaks associated with aromatic and cyclic species, consistent with the known typical composition of aviation kerosene.

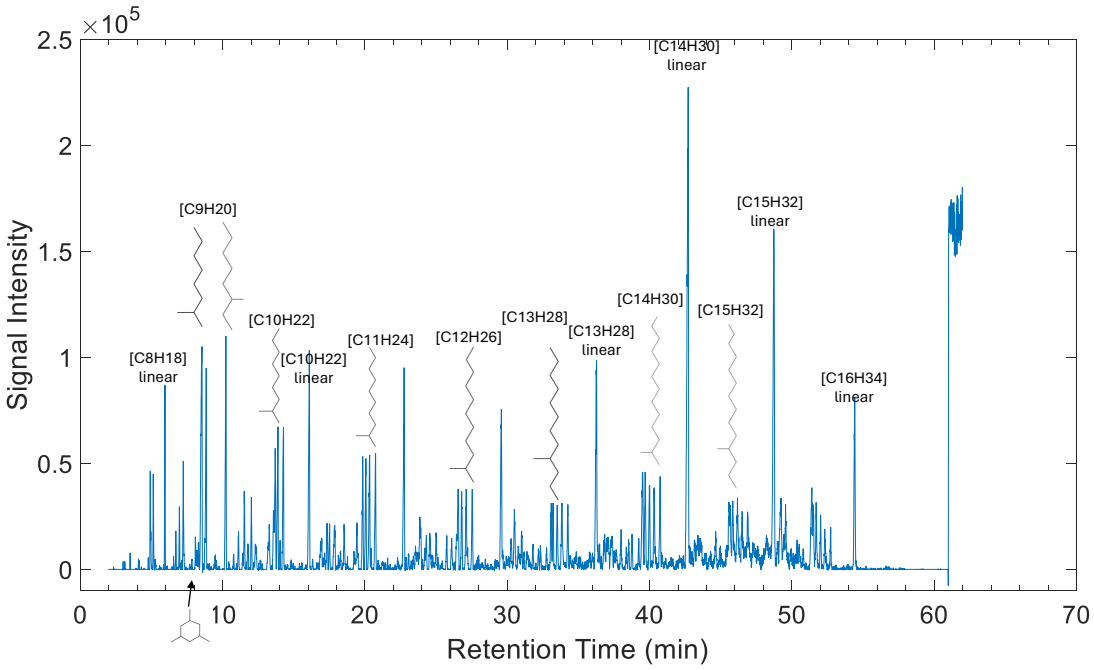

***Fig. 6**: Field ionization signal of SPK*

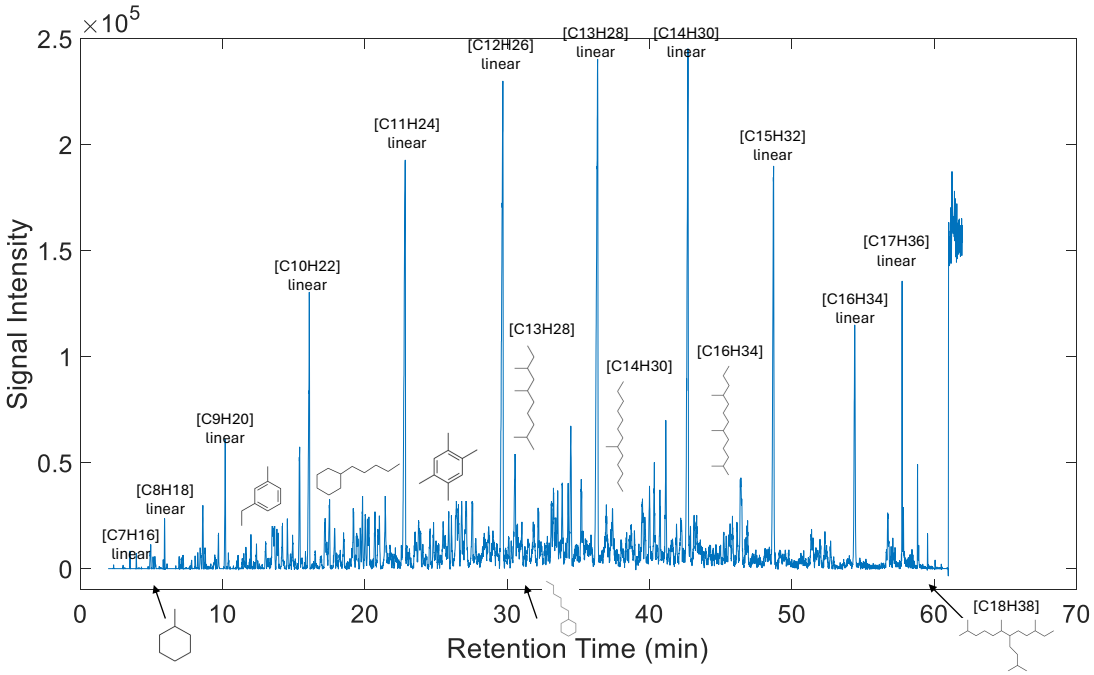

***Fig. 7**: Field ionization signal of Jet A*

A Kendrick Mass Defect (KMD) analysis was conducted on the field ionization (FI) signals using the Mass Mountaineer v7.1.13.0 software to reach a global visualization of the fuels composition. Outcomes provide the relative abundance of the different molecular families composing the tested fuels. The resulting Kendrick plots of Jet A and SPK are compared in Figure 8. Each dot corresponds to one group of molecules with a given KMD value (y-axis), directly linked to the molecular family, and a molecular mass (x-axis). The amplitude of the dot represents the sum of the signal amplitudes from

the FI data of the molecules included in the group. Each molecule group has its own KMD value and can be recognized in the plot. The observed ion intensities do not reflect absolute concentrations because of differences in the ionization efficiencies among the various classes of hydrocarbons. Standard calibration plots could not be made for each molecule identified in the analysis. Therefore, the results cannot provide absolute values of molecule concentration, but they provide a good relative comparison when two fuels are analyzed under the same experimental conditions. The molecule families detected in each fuel are gathered in Table 3. It appears from the KDM plots that Jet A and SPK share a very similar composition regarding the alkanes. The SPK contains only alkanes and a few cyclic alkanes and alkenes. Jet A contains a more diverse range of molecules. The SPK has carbon molecules up to C16, while Jet A has carbon molecules up to C19 with temperature programs used in the GC.

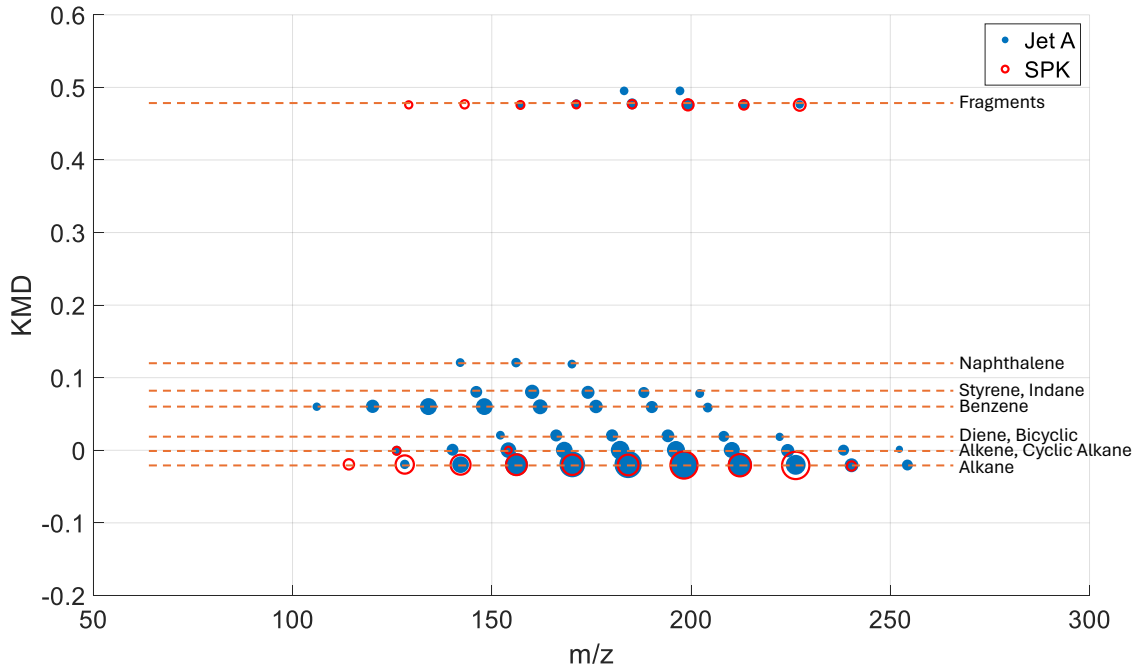

***Fig. 8**: Kendrick mass defect plots of Jet A and SPK*

***Table 3**: Relative abundances of the different molecule families, obtained with the Kendrick Mass Defect method*

Molecule Family	**POSF-4658**	**SPK**
Alkane	Presence	Presence
Alkene, Cyclic Alkane	Presence	Presence
Diene, Bicyclic	Presence	-
Benzene	Presence	-
Styrene, Indane	Presence	-
Naphthalene	Presence	-

3 Results and discussion

3.1 Test Repeatability

AIT test repeatability is assessed by conducting ignition tests at experimental conditions that are as similar as possible from one to the other. The temperature signals from T4 can be separated into two phases: the first few seconds of the signal during the fuel injection and the later temperature peak during ignition. Results are illustrated by three Mode I ignition tests at 217°C with 75 μL of SPK injected. Details of the temperature signals are given in Figure 9 and 10 for the ignition and the injection phase, respectively. The exothermic reaction starts at the same moment for the three tests, at around 115 s, where a faster temperature increase can be seen. The temperature increases similarly for all tests until the ignition, which appears between 127 and 133 seconds after injection. The shape of the temperature signal is similar for the three cases. To highlight the similarities, the integral of the signal has been calculated from 115 and 150 s. Results of the signal processing are gathered in Table 4. Repeatability of the injection is challenging, even with an automatic injection system, as shown in Figure 10. The temperature variation observed at the beginning is due to the cold needle entering and leaving the flask and does not appear to be primarily caused by vaporization as observed by other authors (Chen and Hsieh (2010), Johnson and Mashuga (2023), Setchkin (1954)). The temperature of the flask is affected by the injection and takes 3 to 60 seconds to stabilize after injection.

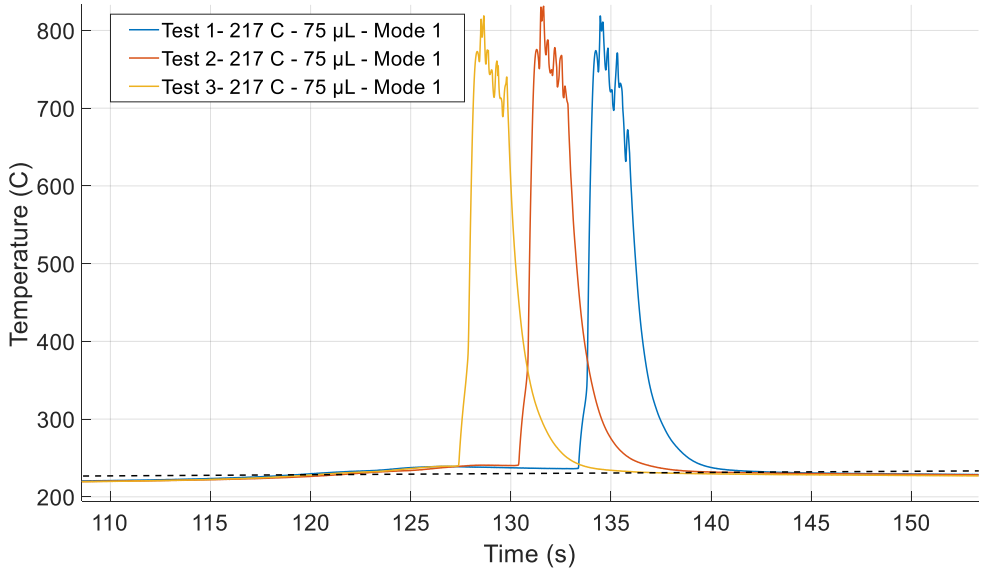

***Fig. 9**: Test sensitivity and repeatability, temperature signals during the ignition - SPK*

***Table 4**: Characteristics of ignition tests at 217°C, 75 µL, SPK*

Test	Ignition time	Maximum temperature	Integral temperature peak
1	133.4 s	818.7°C	1.06e4 C·s
2	130.4 s	831.1°C	1.06e4 C·s
3	127.4 s	818.8°C	1.05e4 C·s

3.2 Ignition Testing Results

The ignition test results for the SPK and Jet A are shown in Figures 11 and 12. Configuration 1 of the ASTM test (see Section 2.1) was used for the SPK data, which were all acquired during the present

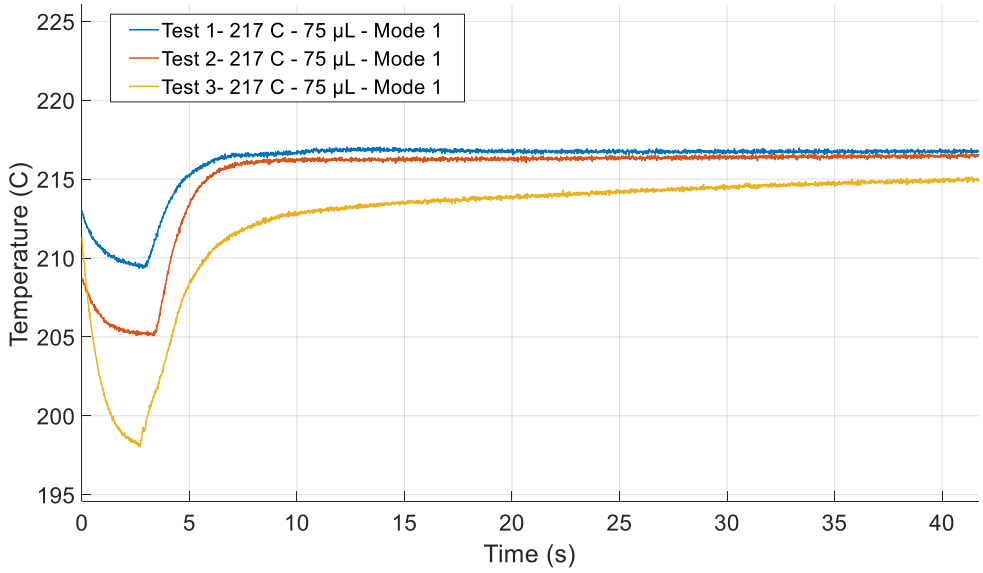

***Fig. 10**: Test sensitivity and repeatability, temperature signals during the injection - SPK*

study. The difference between the ignition maps obtained with Configurations 1 and 2 is discussed in Section 3.6. No flame was visible in Mode III ignition when testing the SPK fuel. However, a noticeable flow from the vessel and a small puff of smoke was observed at the time of ignition. Jet A results from the present study and those of Martin and Shepherd (2021) are plotted together. Consistency is observed between the two sets of measurements.

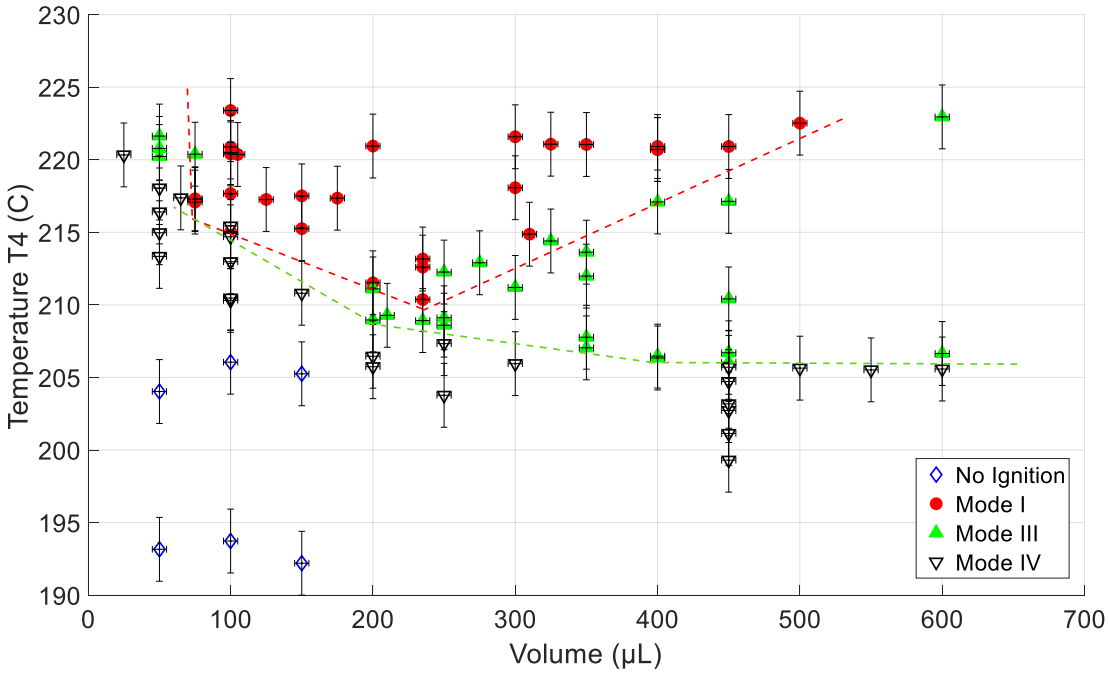

***Fig. 11**: SPK ignition testing results - Configuration 1*

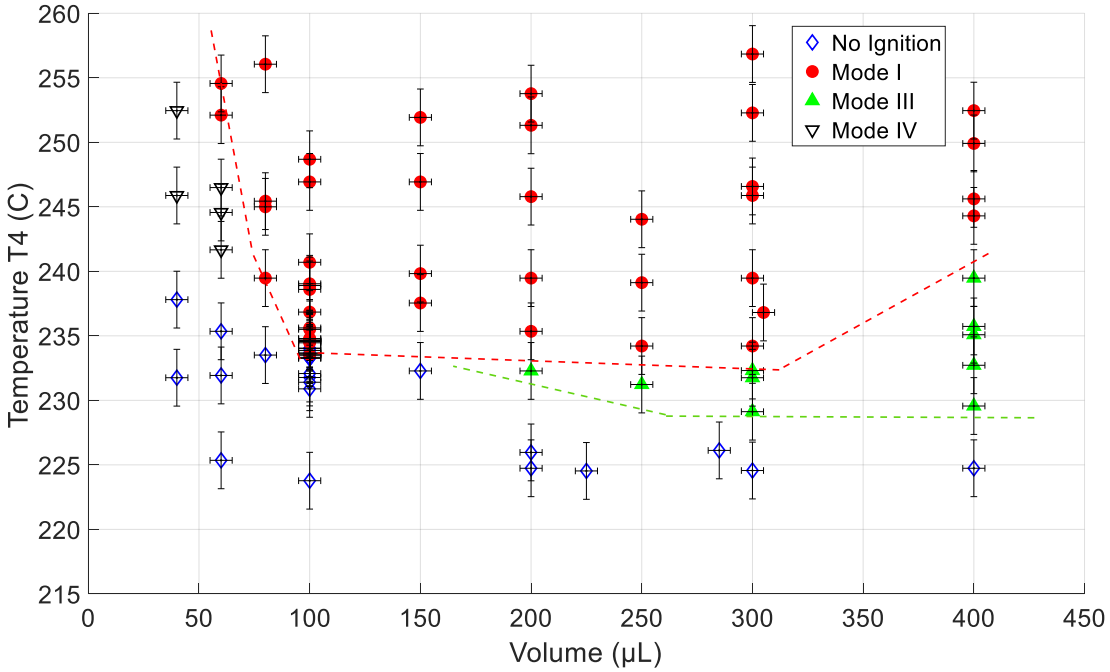

***Fig. 12**: Jet A ignition testing results. Ten tests from the present study (Configuration 1) are shown together with the data from Martin and Shepherd (2021).*

Three ignition modes are observed for both fuels. Figure 13 gives examples of T4 temperature signals obtained from Mode I, III, and IV at various experimental conditions for SPK. While Mode III presents the absence of a visible flame, compared with Mode I, the temperature signals cannot be distinguished between these two modes. However, temperature signals observed during Mode IV event are very different from Modes I and III, with much lower temperature rises and larger ignition delay times. Figure 14 gives the maximum temperature recorded from T4 during the tests, as a function of the initial temperature. The different modes are represented by different markers and colors. White dots have been added to the markers representing the data from Configuration 2. A clear demarcation is observed between Mode IV and Mode III. However, the transition between Mode III and Mode I is smooth, with an overlap between the two modes in a specific temperature range.

Our observations lead to the conclusion that the modes can be separated into two groups - the non-ignition group, with Mode IV and No ignition, where the temperature rise during the chemical reaction is negligible compared to the initial air temperature, and the ignition group, with Mode III and Mode I, where the temperature rise is large enough to create potential hazards by initiating a propagating reaction. The similarities between Mode I and Mode III have already been discussed in the past (Martin and Shepherd, 2021, Johnson and Mashuga, 2023). Based on the experimental observations, we propose to characterize the AIT of a tested fuel based on temperature signals and not flame luminosity and use the Mode III and I ignition events to define the AIT instead of just Mode I.

Dashed lines on Figures 11 and 12 represent the approximate low limits of Modes I and III. The minimum of the two boundaries occurs at different injected volumes and temperatures. It was observed for both fuels that the lower limit of Mode III occurs at higher fuel volumes. A minimum in the lower limit of the Mode III region has not been determined in our tests. Tests at larger fuel volumes will be necessary to investigate if such a minimum exists.

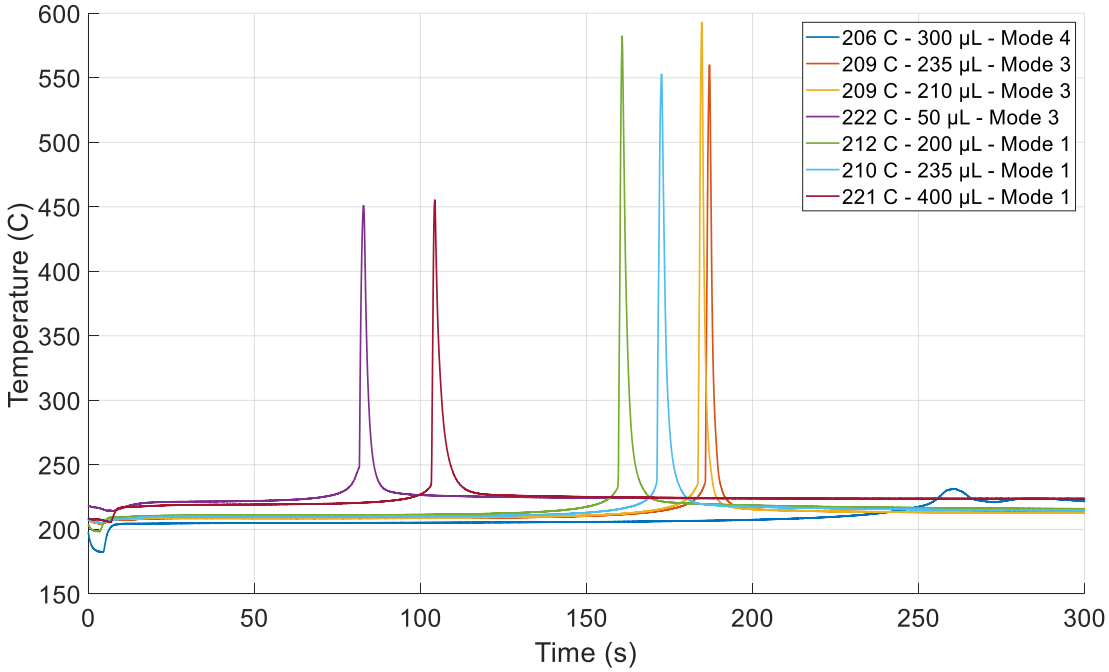

***Fig. 13**: Temperature signals for different ignition modes - SPK*

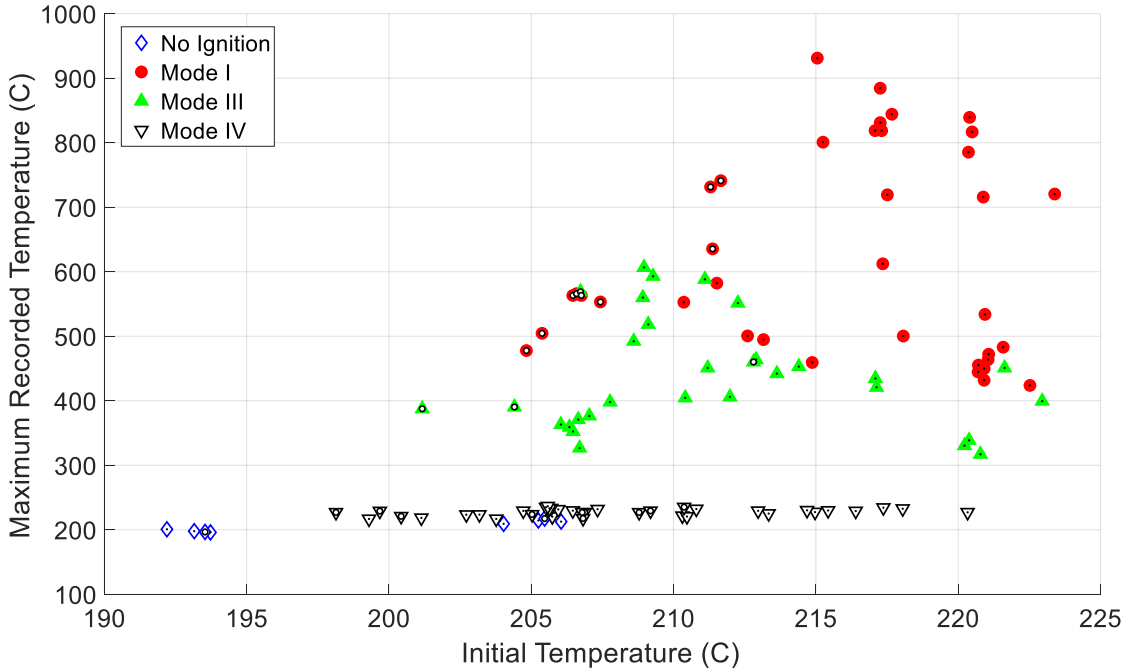

***Fig. 14**: Maximum temperature recorded as a function of the initial test temperature - SPK*

Lines between the different Modes allow better visualizations of the ignition limits but can be deceptive. The transition between no ignition and ignition is not a straight line and can spread over a temperature interval. This phenomenon is discussed in more detail in Sections 3.4 and 3.5.

3.3 Ignition Characteristics

The ignition delay time has been investigated as a function of the initial temperature of T4. The time is plotted in logarithmic scale as a function of the inverse of the initial temperature in Figure 15 for SPK. All the tested fuel volumes are represented for ignition modes I and III. The two ASTM configurations have been used in this study. The markers with a white dot represent data from Configuration 2. The others are from Configuration 1.

A linear correlation can be found by using the Arrhenius plot of the logarithmic value of the ignition time and the inverse of the initial temperature for the two sets of data. While the ignition delay time for these tests is known to depend on the mixture composition (Babrauskas, 2003), our measured ignition delay times appear to depend primarily on the initial temperature. The slopes of the two linear correlations are very similar, and only a small shift in the intercept is observed. An overlap of the curves is obtained when the reference temperature of Configuration 2 is shifted by 2°C. The experimental ignition delay time τ_i can be modeled as:

$$\tau_i = ae^{b/T}, \tag{1}$$

with a and b empirical constants obtained by carrying out linear regression for $\ln \tau_i$ vs T^{-1}. The values are $b = 1.4\times10^4$ K^{-1}, and $a = 4.3\times10^{-11}$ s for Configuration 1; $a = 3.85\times10^{-11}$ s for Configuration 2 and b has the the same value as Configuration 1.

Our results are consistent with a simple Arrhenius form of a one-step model reaction and the Semenov/Frank-Kamenetskii model for the ignition delay time (Babrauskas, 2003):

$$\tau_i \propto e^{Ea/(\tilde{R}T)}, \tag{2}$$

where Ea is the effective activation energy of the tested fuel, and $\tilde{R}$ the universal gas constant.

The effective activation energy of the tested SPK can be computed from the constant b of the regression analysis and is equal to:

$$Ea_{\mathrm{SPK}} = 116\ \mathrm{kJ\cdot mol^{-1}} \quad \text{or} \quad 28\ \mathrm{kcal\cdot mol^{-1}}. \tag{3}$$

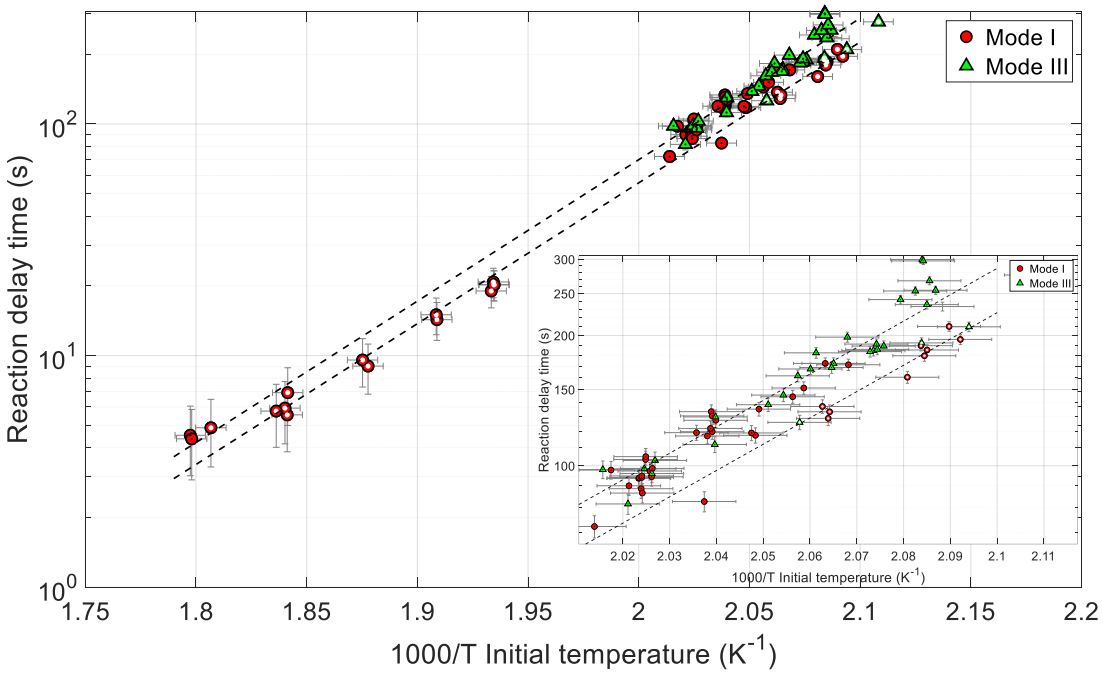

***Fig. 15**: Reaction delay time as a function of initial temperature - SPK*

The same analysis has been conducted with Jet A. The data are gathered in Figure 16. The effective activation energy of the tested Jet A is estimated as:

$$Ea_{\text{Jet A}} = 141\ \text{kJ}\cdot\text{mol}^{-1} \quad \text{or} \quad 34\ \text{kcal}\cdot\text{mol}^{-1}\,. \tag{4}$$

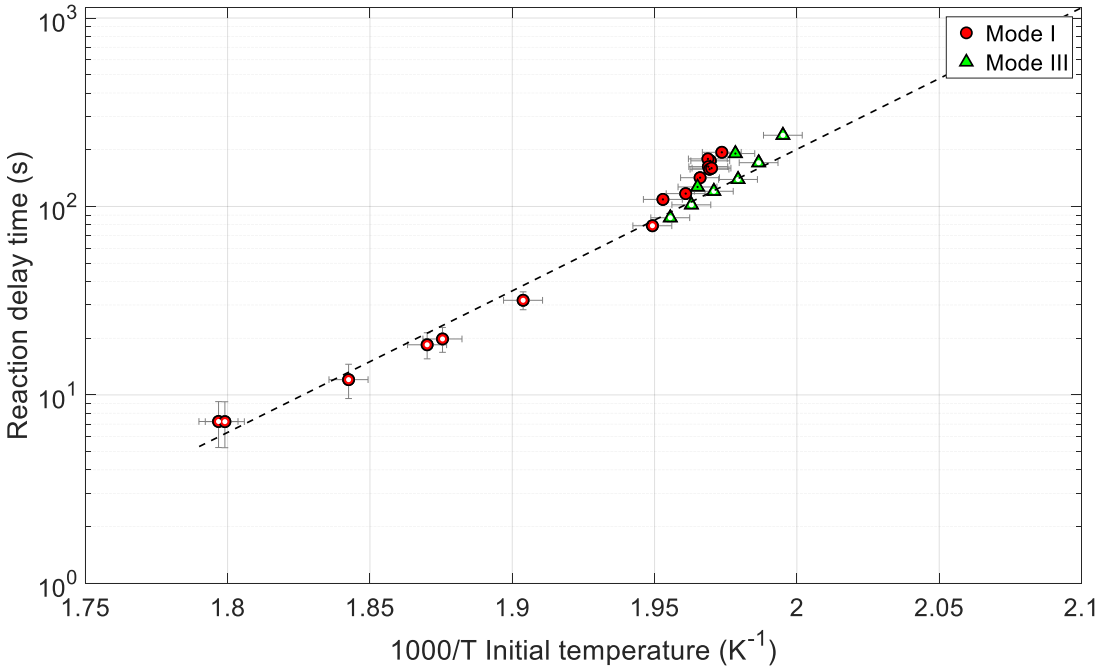

***Fig. 16**: Reaction delay time as a function of initial temperature - Jet A*

A common feature of reaction delay time data is that the Arrhenius plots are not linear, and the effective activation energy depends on the temperature and pressure. A general trend (Babrauskas, 2003) is that Arrhenius plots for autoignition exhibit at least two slopes, i.e, two effective activation energies; one at high temperature (with $Ea \approx 50$ to 90 kJ·mol^{-1}) and one at low temperature (with $Ea \approx 140$ to 190 kJ·mol^{-1}). The low-temperature range of values is consistent with our experimental results and similar in magnitude to the range of values reported in the literature (Goodger and Eissa, 1987, Lefebvre et al., 1986, Babrauskas, 2003) for paraffin-based fuels.

The effective activation energy is a useful way to summarize the fuel ignition delay and is widely used in simplified models of ignition. However, the value obtained is highly dependent on the testing environment and fuel type and is not a true measure of chemical reactivity but depends on the many complex phenomena involved before and during ignition, such as heat transfer, turbulence, and fuel vaporization, and does not account for composition changes during combustion. The value is qualitative and can be carefully compared for different fuels only tested in the same environment.

The variation of the maximum temperature recorded during ignition has been studied as a function of the injected fuel volume. Figure 17 gathers the collected data for SKP. White dots highlight data from ASTM Configuration 2. The other markers are from the ASTM Configuration 1. The temperature dependence regarding the fuel volume is not apparent for the non-ignition and Mode IV cases. Mode I and III ignitions present a temperature peak at around 100 μL. Ignition with that specific fuel volume leads to the most violent combustion reactions with the highest temperature. It is suspected that 100 μL represents a volume near the stoichiometric conditions. Mode I and Mode III cannot be distinguished regarding their behaviors. The same trend is observed for Jet A. Data for Jet A are gathered in Figure 18.

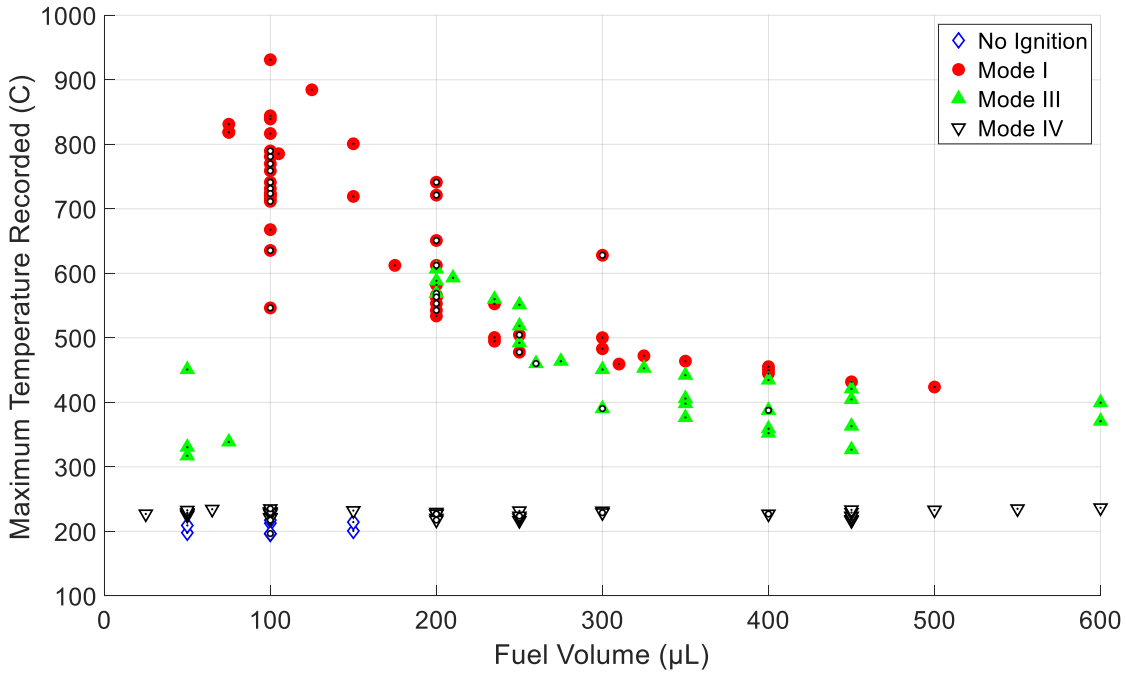

***Fig. 17**: Maximum temperature recorded as a function of the injected fuel volume - SPK*

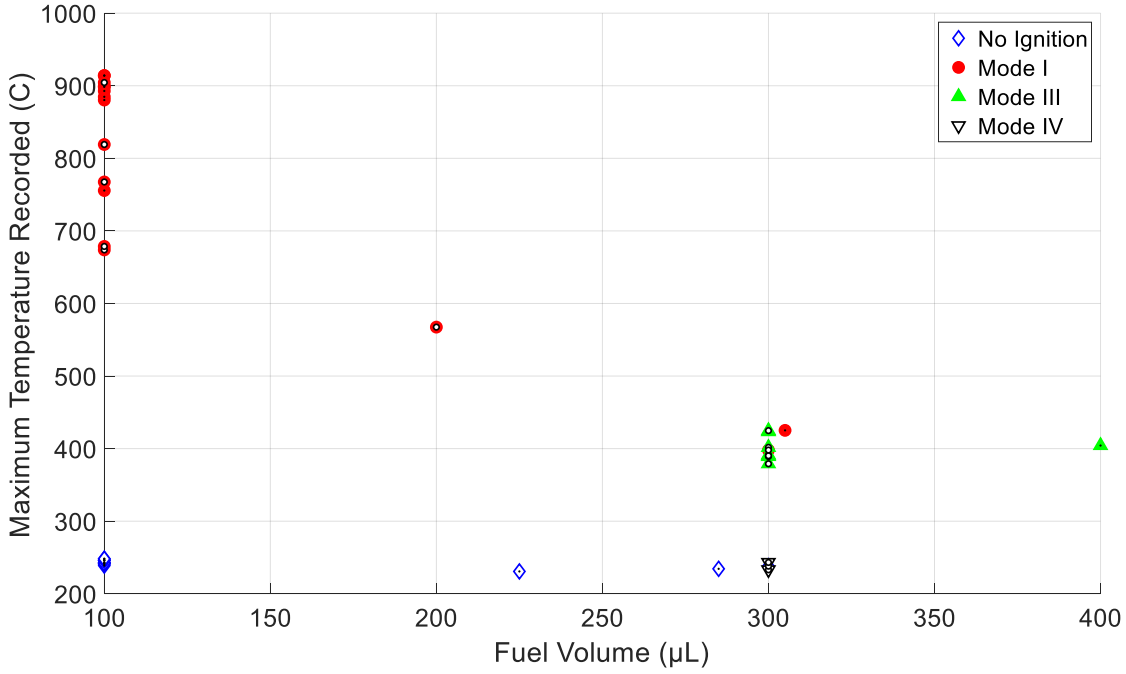

***Fig. 18**: Maximum temperature recorded as a function of the injected fuel volume - Jet A*

3.4 Ignition Transition

The transition between the different ignition modes is investigated by analyzing the different temperature signals at different temperatures for an equal fuel volume. Figures 19 and 20 give the temperature signals of 50 μL and 450 μL of SPK, respectively. When a small amount of fuel is injected (here 50 μL), the temperature signal at a temperature just before the transition between no-ignition (Mode

IV) and ignition (Mode III) is composed of one smooth temperature bump (see signal at 218°C, 50 μL). More complex phenomena occur when the injected volume increases, where multiple peaks can be seen (see signal at 206°C, 450 μL). It was observed that the ignition occurs at the second or third temperature peak (see signal 207°C, 450 μL). This two to three-stage reaction seems typical to some transportation fuels, as it was also observed in the very first ASTM-style tests by Setchkin (1954) when testing Motor Gasoline. Contrary to his observations, the multiple-stage reaction depends here on the tested fuel volume and happens in rich atmospheres. Once the temperature is high enough, the signal is only composed of one peak, as for the lower fuel volume cases.

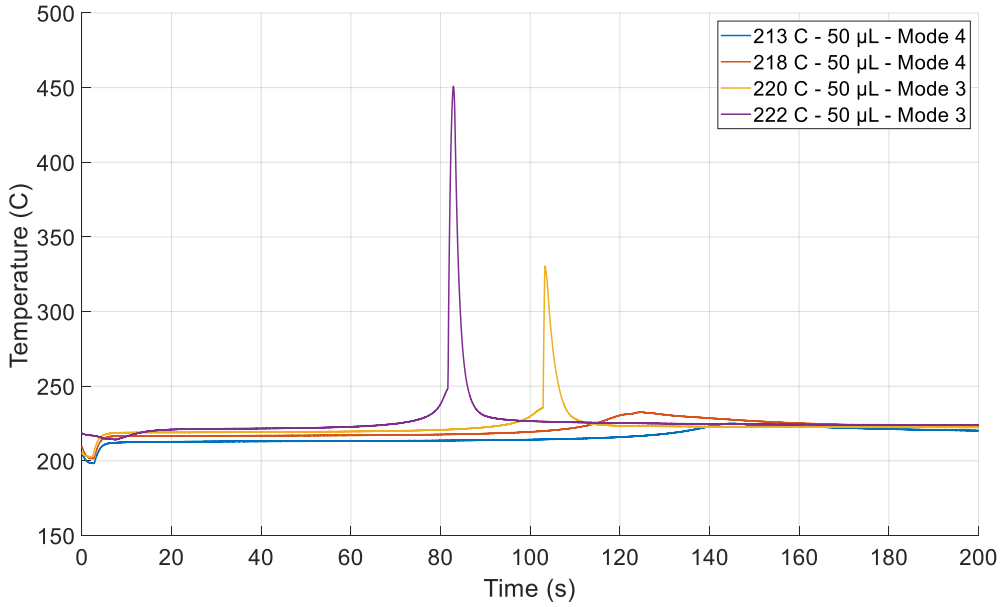

***Fig. 19**: Transition between Mode III and Mode IV, SPK, 50 µL*

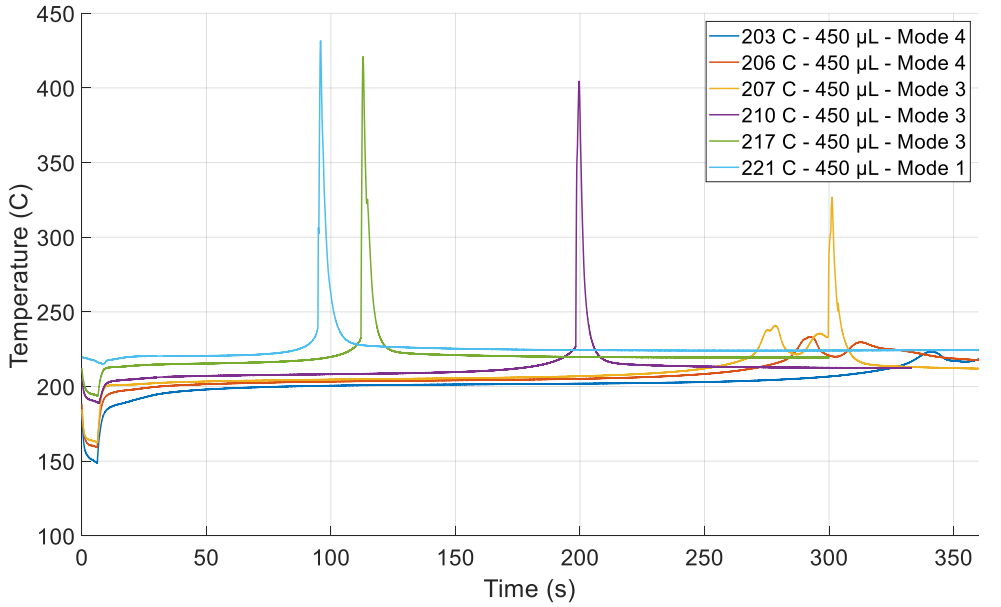

***Fig. 20**: Transition between Mode I, Mode III, and Mode IV, SPK, 450 µL*

Figure 21 examines the transition between non-ignition and ignition, showing a close-up comparison

of two tests conducted at the same temperature for two different fuel volumes. Interestingly, the two temperature signals present a similar temperature increase at the beginning of the exothermic reaction just after 150 seconds. A switch occurs several seconds later when the 200 μL ignites while the 150 μL does not.

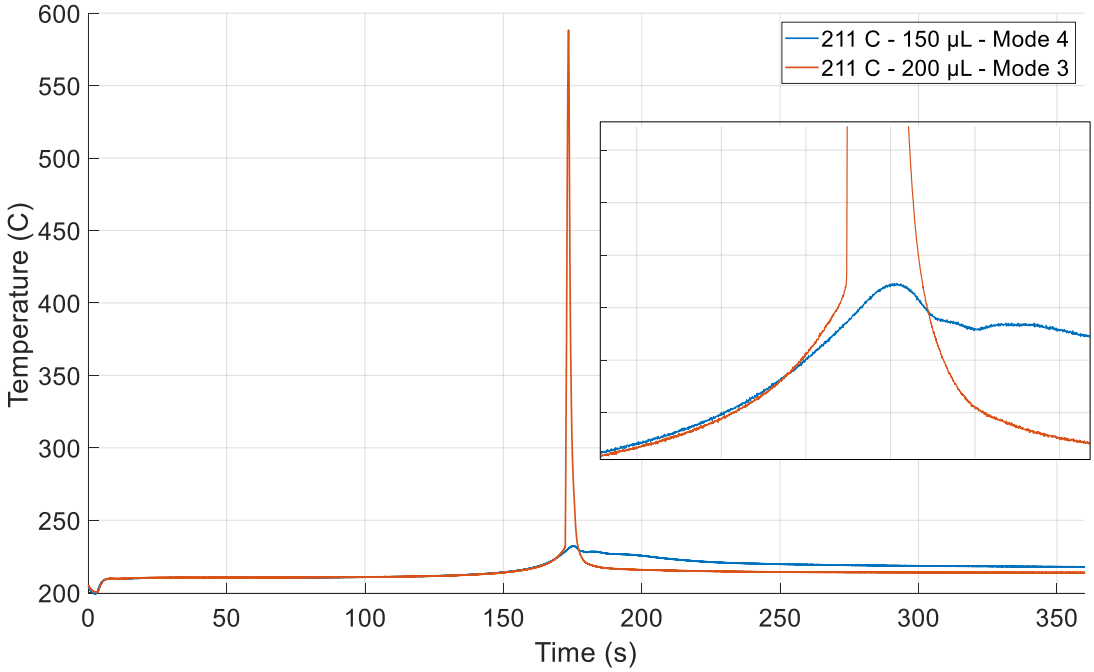

***Fig. 21**: Transition between Mode IV and Mode IV, SKP*

As discussed by Martin (2023), and similarly to dust cloud ignition (Danzi et al., 2018) or spark ignition (Bane et al., 2013), the transition between no ignition and ignition of a fuel in a hot atmosphere is not a sharp line and a zone where both cases can occur exist. The nature of this transition region is discussed in the next section.

3.5 Ignition Statistical Analysis

The statistical methodology of logistic regression (Hosmer and Lemeshow, 2000) was applied to two data sets, one from the Jet A testing and the other from SPK testing. The data from the previous testing series (Martin, 2023) used Configuration 2; data from the present tests used Configuration 1. In this study, we consider both Mode I and Mode III as ignition events.

A total of 80 results for a standard sample (POSF 4658) of aviation kerosene were analyzed with the logistic regression technique. The majority (70) were from previous testing series (Martin and Shepherd, 2021), and 10 were added from the present round of testing. The results are shown in Figure 22 (right) as a plot of the outcomes y_i vs. the temperature T at the center of the test vessel. For clarity, the data points have been randomly displaced from the ignition (y = 1) and non-ignition (y = 0) axes. The confidence intervals were computed in terms of the stimulus $x(\pi)$ using confidence limits in the logit function for a particular value of $\hat{\pi}$

$$\frac{1}{\hat{\beta}_1}\left(\hat{g}(x) \pm z_{\alpha/2}\hat{\sigma}_{\hat{g}(x)} - \hat{\beta}_0\right) = x(\hat{\pi}) \pm \frac{1}{\hat{\beta}_1} z_{\alpha/2}\hat{\sigma}_{\hat{g}(x)} \tag{5}$$

using the approach discussed in Hosmer and Lemeshow (2000). The symbol π denotes the probability of ignition and x corresponds to the temperature $T4$. Symbols with a hat, such as $\hat{\pi}$, $\hat{\beta}$, etc., are expected values computed using the maximum likelihood method.

Note that this analysis uses the aggregate of all test conditions, which spans a range of 50 to 400 μL in fuel volume in addition to the range of temperatures shown. This approach introduces additional factors, fuel volume and ignition mode, which could be included in the regression analysis, but we lack sufficient points at each volume and mode to discriminate between these factors. We elected to focus on temperature as the most important variable. We acknowledge that this differs from the procedure of ASTM-E659 (2005), but as the fuel concentration is unknown in most hazard situations, we propose that this method enables an assessment of ignition threshold that includes variability in fuel concentration and only includes modes with a significant temperature rise as an ignition.

A total of 61 data points are located in the overlap region between 229 and 246°C. The uncertainty limits shown on each datum are ±2.2°C which is the stated accuracy uncertainty of the type K thermocouple used in the apparatus. The precision is much greater, the standard error of the mean is on the order of ±0.1°C and limited by signal fluctuations and record lengths used to obtain mean values.

A useful way to summarize the results with a single statistic is the temperature where $\hat{\pi} = 0.5$, the temperature T_{50} that corresponds to 50% likelihood of ignition. From the logistic analysis, the stimulus at a particular value of expected probability is

$$x(\hat{\pi}) = \frac{1}{\hat{\beta}_1}\left[\ln\left(\frac{\hat{\pi}}{1-\hat{\pi}}\right) - \hat{\beta}_0\right].$$

The value of $T_{50} = -\hat{\beta}_0/\hat{\beta}_1$ for the Jet A data in Figure 22 is 233.4°C and the 95% confidence interval is 5.7°C.

The effect of temperature measurement uncertainty was assessed by carrying out a Monte Carlo study of the effect of random variation of the measured temperatures on the computed value of T_{50}. Random deviates were sampled from a normal distribution with a standard deviation of 2.2°C and added to each temperature in the data series. Random sampling, perturbation of the temperatures, and logistic analysis was repeated 5000 times. The frequency of T_{50} values was recorded, see Figure 23 and analyzed. The distribution is approximately normal, the peak frequency is 233°C and 95% of the data are within ±1.1°C, which is substantially smaller than the confidence interval obtained from the logistic regression on the original data set.

A total of 71 results from the ASTM E659 tests for a sample of synthetic paraffinic kerosene (SPK) were analyzed with the same logistic regression technique as used for Jet A. The results are shown in Figure 22 (left). A total of 47 data points are located in the overlap region between 206 and 220°C. The value of T_{50} for the SPK data in Figure 22 is 207.9°C and the 95% confidence interval is 7.8°C. The effect of temperature measurement uncertainty was assessed by carrying out a Monte Carlo study of the effect of random variation of the measured temperatures on the computed value of T_{50}. The frequency of T_{50} values are shown in Figure 23. The distribution is approximately normal, the peak frequency is at 207.9°C and 95% of the data are within ±5.9°C, which is somewhat larger than the confidence interval obtained from the logistic regression on the original data set.

Results from another sample of Jet A, POSF10325, obtained by Martin and Shepherd (2021), are shown to illustrate the range of AIT results possible with different batches of Jet A. The T_{50} temperatures are slightly lower (227.8°C) and the 95% confidence interval (13.5°C) is approximately twice as large. The results of the Monte Carlo study are consistent with these values.

All the results are summarized in Table 5. The temperature for a 50% likelihood of the new SPK is lower than Jet A (POSF4658), and no overlap was observed between the two fuel data sets. These observations highlight a lower, about 20°C, autoignition temperature for the SPK compared to Jet A (POSF4658). Even though the overlap regions where both ignition and no ignition cases can occur have a similar width, Jet A (POSF4658) has a much sharper T_{50} distribution, where the 95% of the Monte Carlo data interval is almost 6 times smaller than the SPK. It is not yet known if this observation is due to the physical properties of the fuel or the distribution of the tested experimental condition. More work is needed to draw a final conclusion on this behavior.

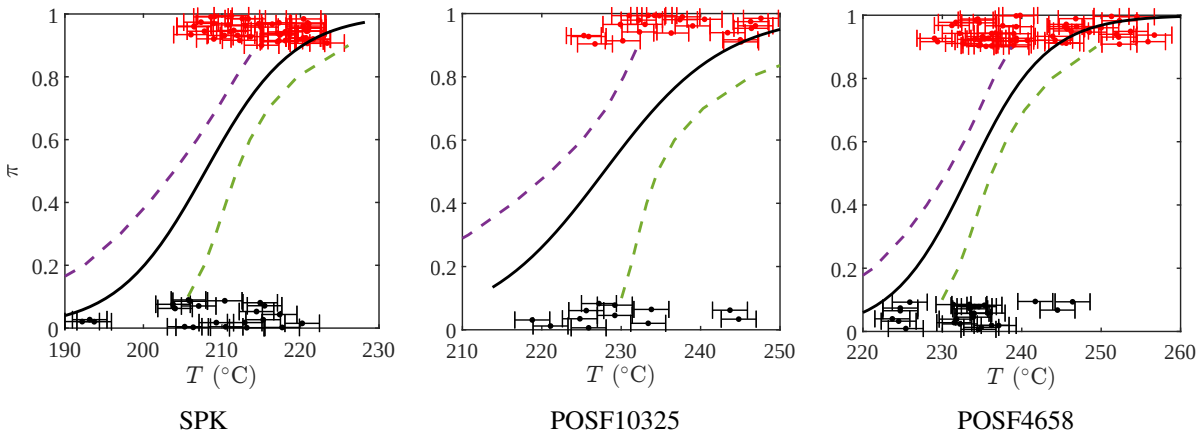

***Fig. 22**: Logistic analysis of ASTM E659 test results for a synthetic paraffinic hydrocarbon (SPK) and Jet A (POSF10325, POSF4658). The solid line is the MLE estimate of probability and the dashed lines are the 95% confidence interval.*

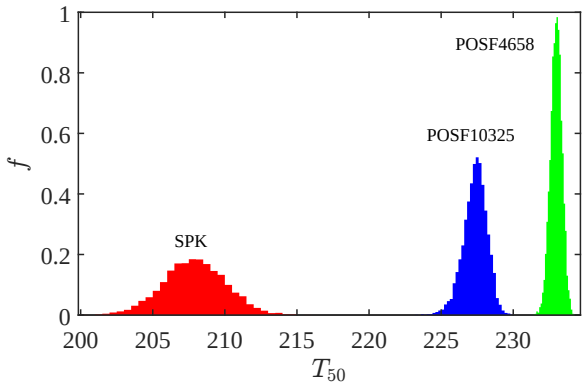

***Fig. 23**: Frequency of T_{50} values computed from 5000 logistic analyses of SPK and Jet A data simulating the effect of uncertainty in measured temperature.*

3.6 Effect of the ASTM Apparatus and Estimation of an AIT Value

The ignition map for SPK was initially generated with Configuration 1 of the ASTM apparatus (see Section 2.1). Results from Configuration 2 have been added on Figure 24 for SPK. The new data are highlighted by white dots and the uncertainty bars of only the new data have been kept on the graph to enable visibility.

The new data shows a shift a few degrees down compared to the old data. Users shouldn't interpret these results as indicating a lower AIT or a lack of repeatability but rather as an issue with characterizing the temperature inside the flask. The ASTM protocol uses one-point measurement as the temperature reference. One key issue is the use of this temperature reference to directly estimate the AIT temperature temperature directly. The measurement of the temperature profile inside the flask for the two configurations (Figure 3) shows that a small apparatus modification can lead to a significant difference in temperature distribution. In the presented case, a variation of 3% between T4 and the temperature over the vertical profile was estimated for the two configurations. This variation represents a difference of more than 6°C, which is slightly higher than the shift observed on the new ignition map. This observation is consistent with the idea that T4 is inadequate at characterizing the initial temperature conditions inside the flask and that more accurate AIT measurements could be reached with a better temperature reference. In order to have better accuracy in the AIT estimation, the temperature distribution inside the flask needs to be characterized accurately and a standardized temperature uniformity needs to be defined, which is not yet the case in the standardized protocol.

***Table 5**: Summary of the logistic regression and Monte Carlo analyses*

Fuel	Overlap Region	Overlap Width	T_{50}	95 % Confidence Interval	MC Peak Frequency T_{50}	95 % of the MC Data
SPK	[206 220]°C	14°C	207.9°C	7.8°C	207.9°C	±5.9°C
POSF10325	[225 245]°C	20°C	227.8°C	13.5°C	227.4°C	±2.2°C
POSF4658	[229 246]°C	17 °C	233.4°C	5.7°C	233°C	±1.1°C

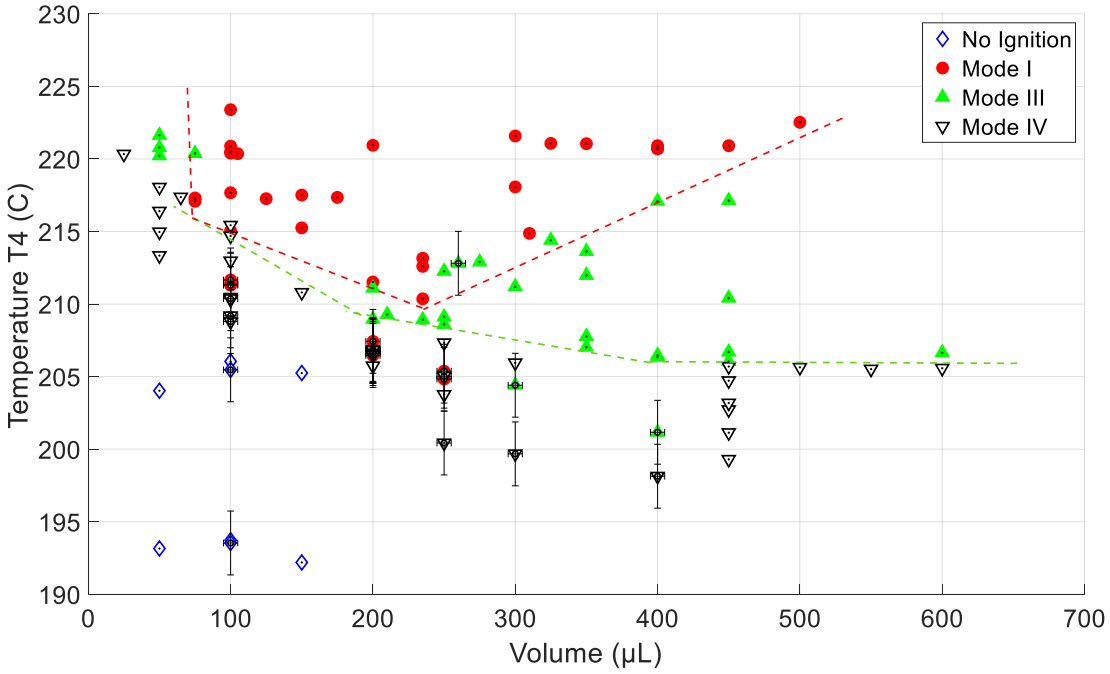

***Fig. 24**: SPK ignition testing results for two configurations. Configuration 1 data are without error bars, Configuration 2 are with error bars and white dots in markers.*

Another key issue is that AIT values given in the literature are associated with a particular temperature distribution, which is usually not reported. In our case, the temperature profile of Configuration 1 provides an estimation of a variation of temperature inside the flask of 3%. This is under the assumption that the temperature inside the whole flask is represented by its centerline profile and that this variation is consistent over the range of test conditions. Further analysis needs to be conducted to investigate the temperature distribution inside the flask and its variation compared to the value given by T4 in order to estimate the AIT of the tested fuels with more confidence.

4 Conclusions

The ASTM-E659 standard has been used to investigate the autoignition of two fuels: Jet A-POSF4658 and a representative Synthetic Paraffinic Kerosene (SPK). The two fuels present a similar composition regarding the alkanes but unlike Jet A, the SPK is mainly composed of alkanes, with just a few alkenes and cylco-alkanes, and no aromatics. An automatic injection system has been used to improve the repeatability of the tests. A higher resolution for temperature acquisition than the one used in the ASTM standard has also been used so that the reaction delay times of the two fuels could be investigated as a function of the initial temperature. The results were fitted to a simple Arrhenius model, and an effective activation energy was computed.

The ignition maps of the two fuels have been given and discussed. Results highlight the importance of using the digital recording of the small gauge thermocouple to detect and quantify ignition instead of

relying only on flame visualization, as suggested by the standard. Mode III ignition (no flame) appears as vigorous (comparable temperature excursion) as Mode I (flame) but often occurs at a lower initial temperature. For this reason, in our statistical evaluation, we consider both Mode I and Mode III to be ignition events.

Autoignition testing under the ASTM protocol aims to define a sharp limit between no-ignition and ignition corresponding to the AIT. Our results show the existence of a temperature interval where both ignition and no-ignition events can happen. In our study, ignition occurs in a temperature interval of 15-20°C and can be characterized by the 50% probability of ignition and a confidence interval.

The autoignition temperature of our SPK sample was found to be 20-25°C lower than Jet A using either statistical or conventional methods to define the ignition threshold temperature. The ignition processes were very similar in the two fuels, with the absence of Mode II ignition, the presence of multiple peaks for large tested fuel volumes, and the general aspect of the ignition maps.

The temperature distribution inside the flask was found to influence the outcome of autoignition testing. We observed that a slight modification of the ASTM apparatus can significantly change the temperature distribution. Using a single thermocouple in the middle of the flask without considering the temperature distribution can lead to erroneous estimations of the AIT and its associated uncertainty. An effort has been made in this project to distinguish the temperature measured by the thermocouple T4 from the AIT value. Future studies are planned to characterize the effect of temperature distribution on ignition thresholds and the implications of reporting AIT values.

Acknowledgements

This research was carried out in the Explosion Dynamics Laboratory of the California Institute of Technology. This work was supported by The Boeing Company through a Strategic Research and Development Relationship Agreement CT-BA-GTA-1 and C. Fouchier was supported by the European Union through a Marie Sklodowska-Curie Fellowship. The authors thank Mona Shahgholi, Manager of The Mass Spectrometry Facility at the Chemistry and Chemical Engineering department of Caltech, for her support and essential help on the fuel composition analysis.

References

Affens, W., Johnson, J., Carhart, H. (1961). *Effect of chemical structure on spontaneous ignition of hydrocarbons.* Journal of Chemical and Engineering Data, 6(4):613–619.

ASTM-D56 (1999). *Standard test method for flash point by Tag closed tester*. American Society for Testing and Materials.

ASTM-E659 (2005). *Standard test method for autoignition temperature of liquid chemicals*. American Society for Testing and Materials.

Babrauskas, V. (2003). *Ignition handbook: Principles and applications to fire safety engineering, fire investigation, risk management and forensic science*. Fire science publishers.

Bane, S., Ziegler, J., Boettcher, P., Coronel, S., Shepherd, J. (2013). *Experimental investigation of spark ignition energy in kerosene, hexane, and hydrogen*. Journal of Loss Prevention in the Process Industries, 26(2):290–294.

Brandes, E., Hirsch, W., Stolz, T. (2018). *Zündtemperaturen in anderen oxidationsmitteln als luft*. PTB-OAR.

Chen, C.-C., Hsieh, Y.-C. (2010). *Effect of experimental conditions on measuring autoignition temperatures of liquid chemicals*. Industrial & engineering chemistry research, 49(12):5925–5932.

Danzi, E., Bibbona, E., Di Benedetto, A., Sanchirico, R., Di Sarli, V., Marmo, L. (2018). *A statistical approach to determine the autoignition temperature of dust clouds*. Journal of loss prevention in the process industries, 56:181–190.

Davis, B., Fouchier, C., Shepherd, J. E. (2024). *Fluid motion and mixing in the ASTM E659 apparatus*. 15th International Symposium on Hazards, Prevention and Mitigation of Industrial Explosions, Naples, Italy, July 10-14, 2024.

Frank-Kamenetskii, D. A. (2015). *Diffusion and heat exchange in chemical kinetics*. Princeton University Press.

Goodger, E., Eissa, A. (1987). *Spontaneous ignition research - review of experimental data*. Journal of the Institute of Energy, 60(443):84–94.

Hirsch, W., Brandes, E. (2005). *Zündtemperaturen binärer gemische bei erhöhten ausgangsdrücken*. Physikalisch-Technische Bundesanstalt, Braunschweig und Berlin.

Hosmer, D. W., Lemeshow, S. (2000). *Applied Logistic Regression*. Wiley Series in Probability and Statistics. Wiley, New York, 2nd ed edition.

ISO/IEC (2017). *Iso/iec 80079-20-1: Explosive atmospheres - part 20-1: Material characteristics for gas and vapor classification-test methods and data*. Technical report, International Orgnization for Standardization.

Johnson, C., Mashuga, C. V. (2023). *Reconsidering autoignition in the context of modern process safety: Literature review and experimental analysis*. Journal of Loss Prevention in the Process Industries, 81:104963.

Jones, S. M., Shepherd, J. E. (2021). *Thermal ignition by vertical cylinders*. Combustion and Flame, 232:111499. Preprint, published version available at `https://doi.org/10.1016/j.combustflame.2021.111499`.

Lefebvre, A. H., Freeman, W. G., Cowell, L. H. (1986). *Spontaneous ignition delay characteristics of hydrocarbon fuel-air mixtures*. Nasa contractor report 175064, NASA.

Martin, C. D. (2023). *Experiments in Thermal Ignition: Influence of Natural Convection on Properties of Gaseous Explosions*. Ph.D. thesis, California Institute of Technology.

Martin, C. D., Shepherd, J. E. (2021). *Low temperature autoignition of jet a and surrogate jet fuel*. Journal of Loss Prevention in the Process Industries, 71:104454.

Mastorakos, E., Baritaud, T., Poinsot, T. (1997). *Numerical simulations of autoignition in turbulent mixing flows*. Combustion and Flame, 109(1-2):198–223.

msFineAnalysis (2023). *Jeol Software, Peabody, MA, USA*. `https://www.jeol.com/`.

NFPA (1991). *Fire protection guide to hazardous materials*. National Fire Protection Association, 10th edition.

Semenoff, N. (1929). *Kinetics of chain reactions.* Chemical Reviews, 6(3):347–379.

Setchkin, N. P. (1954). *Self-ignition temperatures of combustible liquids*. Journal of Research of the National Bureau of Standards, 53(1):49.

Swarts, D. E., Orchin, M. (1957). *Spontaneous ignition temperature of hydrocarbons*. Industrial & Engineering Chemistry, 49(3):432–436.